

18. M. Bowick, A. Cacciuto, D. R. Nelson, A. Travesset, *Phys. Rev. Lett.* **89**, 185502 (2002).
19. We acknowledge support from the China State Key Projects of Basic Research (grant 2002CB613500), the National High Technology Research and Development Program of China (grant 2003AA302170),

and the National Natural Science Foundation of China (grants 60306009, 50472070, and 50272081).

Supporting Online Material

www.sciencemag.org/cgi/content/full/309/5736/909/DC1

Materials and Methods
Figs. S1 to S3

11 April 2005; accepted 23 June 2005
10.1126/science.1113412

A Crossover in the Mechanical Response of Nanocrystalline Ceramics

Izabela Szlufarska,^{1*} Aiichiro Nakano,² Priya Vashishta²

Multimillion-atom molecular dynamics simulation of indentation of nanocrystalline silicon carbide reveals unusual deformation mechanisms in brittle nanophase materials, resulting from the coexistence of brittle grains and soft amorphous grain boundary phases. Simulations predict a crossover from intergranular continuous deformation to intragrain discrete deformation at a critical indentation depth. The crossover arises from the interplay between cooperative grain sliding, grain rotations, and intergranular dislocation formation similar to stick-slip behavior. The crossover is also manifested in switching from deformation dominated by indentation-induced crystallization to deformation dominated by disordering, leading to amorphization. This interplay between deformation mechanisms is critical for the design of ceramics with superior mechanical properties.

The great interest in nanostructured ceramics originates from the observations and expectations of unique mechanical properties (1–3) in these materials. Examples include very high hardness, high fracture toughness, and superplastic behavior in normally brittle ceramics. Silicon carbide is of particular interest because of its potential technological applications in high-temperature structural and electronic components (4). Although enhanced mechanical properties are often associated with the reduction in grain sizes, it has recently been conjectured (5) that nanostructured ceramics might exhibit an inverse Hall-Petch effect; that is, hardness decreases when grain size decreases in the nanoscale grain-size regime. Such peculiar behavior has been observed in ductile nanophase materials (e.g., nanostructured metals) with porous grain boundaries (GBs) by means of simulations (6–8) and experiments (9). The behavior was attributed to a crossover from dislocation-mediated plasticity for large grain size to GB sliding for small grain size (10, 11). A similar mechanistic understanding in ceramics is still lacking.

In contrast with nanostructured metals, nanostructured ceramics have an increased volume fraction of disordered intergranular films, which

are observed both experimentally (12) and by means of molecular dynamics (MD) simulations (13, 14). In particular, for brittle ceramics such as SiC, mechanical properties such as toughness are essentially determined by soft (often amorphous) GB phases (12). Recent experiments (15) of nanoindentation of nanocrystalline SiC (n-SiC) films with grain sizes of 5 to 20 nm have shown “superhardness,” i.e., hardness largely exceeding that of a bulk crystalline SiC (3C-SiC). The experimental hardness was shown to be sensitive to the grain size and the fraction of the amorphous GB phase. However, their effects on mechanical responses at the atomistic level are largely unknown.

The MD simulations consisted of a $625 \times 625 \times 535 \text{ \AA}^3$ n-SiC substrate containing

18.7 million atoms, which had randomly oriented grains with diameters averaging 8 nm and a density of 2.97 g/cm^3 at a temperature of 300 K (16). Structural ordering in GBs is analyzed by means of a partial pair distribution function $g(r)$, which quantifies the probability of finding two atoms at an interatomic distance r . The function $g(r)$ for Si-C pairs is plotted in Fig. 1A (solid line), and it reveals a lack of long-range order, similar to that of bulk amorphous SiC (a-SiC) (dashed line). This is in contrast to a sharp-peak structure of $g(r)$ in a 3C-SiC shown in the inset of Fig. 1A. Visual inspection of the substrate reveals the presence of highly disordered GBs with a more or less uniform thickness. The n-SiC can be thought of as a substrate with two coexisting phases: crystalline inside the grains and amorphous in the GBs. Amorphous GBs were also observed in experimentally sintered n-SiC (17, 18).

To shed light on the atomistic mechanisms underlying mechanical response of n-SiC, we indented the substrate with a square-base indenter of size $160 \times 160 \times 72 \text{ \AA}^3$. Nanoindentation is a unique local probe to measure mechanical properties of materials (19–22). Even though experimental indenters are round on this scale, a square-base indenter helps to maximize the applied stress and the localized plastic flow in the material (23) on length and time scales available to simulations. The resulting load-displacement (P - h) curve is shown in Fig. 1B (solid line), together with two unloading curves (dashed lines). The P - h response exhibits four characteristic regimes.

Regime 1 is entirely elastic and ends at $h = 7.5 \text{ \AA}$. Regime 2 extends up to the crossover depth $h_{\text{CR}} \sim 14.5 \text{ \AA}$ and is characterized by a very small hysteresis during unloading as com-

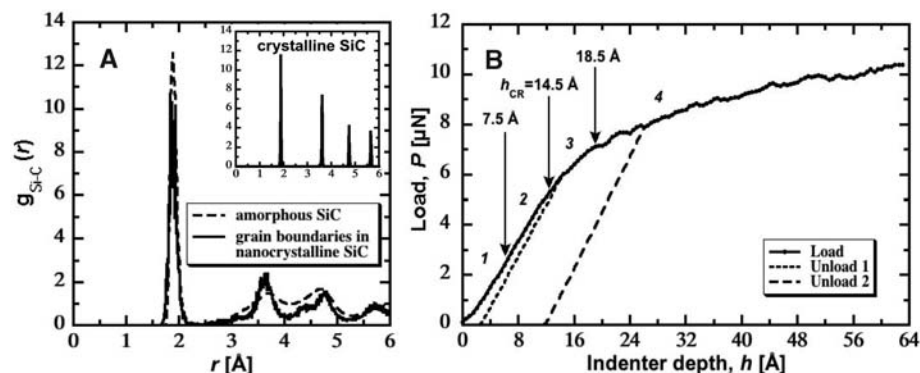


Fig. 1. (A) Si-C partial pair distribution function $g_{\text{Si-C}}(r)$ of GBs in n-SiC (solid line) resembles that of a-SiC (dashed line) in contrast to 3C-SiC (inset). (B) Load-displacement curve of 18.7-million-atom n-SiC, where numbers 1 to 4 mark different regimes in the response. Regimes 1 and 2 are characterized by continuous cooperative grain motion; in regime 3 grains become decoupled from one another; in regime 4 discrete intergrain response is turned on, which is manifested in the small load drops in the P - h curve.

¹Department of Materials Science and Engineering, 1509 University Avenue, University of Wisconsin, Madison, WI 53706–1509, USA. ²Department of Chemical Engineering and Materials Science, 3651 Watts Way, University of Southern California, Los Angeles, CA 90089–0242, USA.

*To whom correspondence should be addressed. E-mail: izabela@engr.wisc.edu

pared with a much more pronounced plastic yield at h_{CR} . The small plastic flow is related to the nonequilibrium structure of the amorphous interfaces, which can relax within a short migration distance (24). A similar effect has been observed during MD simulations of bulk a-SiC (25). Because up to h_{CR} the amorphous “cementlike” GBs hold the grains together, regimes 1 and 2 are characterized by cooperative continuous intergranular response. The cooperative motion of grains is identified by analyzing atomic displacements. It involves both formation of mesoscopic shear planes involving several grains and coupling to grains outside of the area directly beneath the indenter to form an extended elastic zone. Formation of mesoscopic shear planes has been previously observed in MD simulations of nanocrystalline Ni (26).

Regime 3 starts when amorphous GBs yield plastically at $h_{CR} \sim 14.5$ Å and henceforth grains are effectively decoupled from one another. The substrate contains a small number of nanopores, which collapse under the indenter, thereby reducing the yield stress. In experimental nanoceramics, the volume fraction of pores can be as high as 20% (27, 28). The crystalline phase within the grains does not yield until the onset of regime 4 at $h = 18.5$ Å. This response is distinct from that of nanostructured metals, in which a dislocation within the grain is nucleated at the onset of substrate yielding (29–33). Discrete plastic events, such as a dislocation glide, take place within the grains in close proximity to the indenter and are reflected in the rougher character of the P - h curve. Similar periodic load drops have been observed for the nanoindentation in bulk 3C-SiC. In the case of n-SiC, the load drops are much less pronounced than in 3C-SiC (25), because the calculated load is averaged over a few grains covered by the indenter and the discrete events in a grain are decoupled from those in the neighboring grains. The decoupling from grains not lying directly beneath the indenter is shown in Fig. 2A, in which atoms are color coded by ΔR_{CM} , the total displacement of the centers of mass of individual grains from their positions before indentation. The localization of deformation is much more pronounced in regimes 3 and 4 than in 1 and 2.

The crossover from cooperative mechanical response of coupled grains to discrete intergranular events is shown in Fig. 2B, where we plot the average displacement $\langle \Delta r_{CM} \rangle$ of the grains' centers of mass calculated relative to the previous indentation step. The coupling of grains in regime 1 is manifested as the peak of $\langle \Delta r_{CM} \rangle$ at $h \sim 7.5$ Å; in regime 2, the coupling slowly decreases until it becomes negligible at the onset of regime 3. In regime 4 ($h \geq 18.5$ Å), the motion of grains is decoupled and $\langle \Delta r_{CM} \rangle$ oscillates around a constant value of ~ 0.15 Å. The oscillations in $\langle \Delta r_{CM} \rangle$ are correlated with the small load drops in the P - h response. They correspond to the

interplay between the sliding of individual grains, grain rotations, dislocation formation inside the grains, and coupling of grains in the extended elastic zone underneath the plastic one. Examples of discrete plastic events are shown in Fig. 2, C to E. In Fig. 2C, we visualize displacements of atoms at $h = 29$ Å relative to their positions at the previous indentation step. Figure 2, D and E, for $h = 26.5$ and 27 Å, respectively, show a unit dislocation with Burgers vector $\frac{1}{2}[101]$ gliding in the $(\bar{1}11)$ plane through a grain structure containing Shockley partial dislocations and stacking faults (SFs). These SFs exist on every second $\{111\}$ plane below the green line in Fig. 2, D and E, forming a thin bilayer of hexagonal (wurtzite) structure in the face-centered cubic (zinc-blende) structure of crystalline grains. This type of defect is similar to twin boundaries observed in indentation experiments of nanocrystalline aluminum (34), where SFs are formed on the neighboring $\{111\}$ planes. Shockley partial dislocations, SFs, and twins have also been observed experimentally in 3C-SiC (35, 36).

The crossover and localization of deformation are also manifested in the rotation of grains.

Figure 3, A and B, show atomic arrangements in regimes 1 and 4, respectively. To highlight the rotational motions of selected grains, we mark as blue a rectangular box inside the n th grain and calculate its rotation angle $\alpha(n)$ averaged over all atoms inside the box. The standard deviation $\Sigma(n)$ from the mean $\alpha(n)$ is a measure of the grain's deformation. After plastic yielding of the amorphous GBs at h_{CR} , grain 52, lying directly beneath the indenter, experiences a tremendous shear and undergoes both large rotation and deformation (black curves in Fig. 3C). On the other hand, a neighboring grain 71, not lying directly under the indenter, does not rotate or deform during indentation (blue curves in Fig. 3C). This localization of deformation is due to decoupling of grains in regimes 3 and 4. Some of the grains in the indenter vicinity exhibit a behavior similar to stick-slip behavior. For example, grain 36 (red curves in Fig. 3C) shows a sudden jump in rotation $\alpha(36)$ and deformation $\Sigma(36)$ at $h \sim 12$ Å, which is accompanied by a release of accumulated shear stress through a dislocation glide. After the stress has been released, the grain mainly rotates [increasing $\alpha(36)$ and nearly constant $\Sigma(36)$].

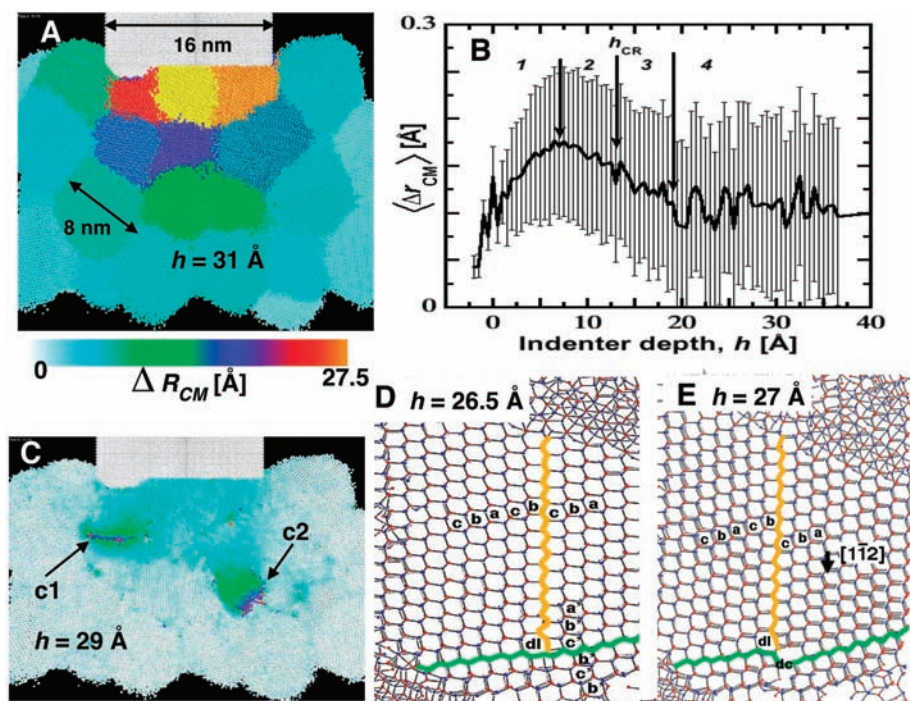


Fig. 2. (A) Grains near the indenter at $h = 31$ Å (regime 4). Atoms are color coded by ΔR_{CM} , the total displacement of grain's center of mass (CM), relative to the initial system. Decoupling of grains results in a pronounced localization of damage beneath the indenter. (B) Mean displacement $\langle \Delta r_{CM} \rangle$ of grains' CMs at every indentation step and its standard deviation. (C) Load drop at $h = 29$ Å is correlated with dislocations gliding inside the grains (c1) and at GBs (c2). Atoms are color coded by their displacement from the previous indentation position. (D and E) The (110) projection of a grain's structure before (D) and after (E) a glide of a unit dislocation with Burgers vector $\frac{1}{2}[101]$ along SF in the $(\bar{1}11)$ plane. The initial structure (D) shows a SF, abcba, along the orange line. The SF is terminated with a Shockley partial dislocation line (dl) along the $[110]$ direction at the boundary (green line) between cubic (zinc-blende) and hexagonal (wurtzite) structure, the latter denoted with the stacking $b'c'b'$. In (E), a black arrow in the $[11\bar{2}]$ direction is a projection of the Burgers vector of the perfect dislocation. After the glide, the dislocation core (dc) becomes pinned at the zinc-blende/wurtzite boundary.

The observed crossover is correlated to a competition between crystallization and disordering in the substrate. To study this effect, we analyzed topological disorders based on the analysis of rings, where a ring is defined as the shortest closed path of alternating Si-C atomic bonds (37). Each atom in a perfect 3C-SiC has 12 unique threefold rings (these are ordered atoms), and a topological disorder is reflected in the presence of rings that are not threefold (disordered atoms). In Fig. 4A, all atoms that remain ordered from the beginning up to $h = 18.5 \text{ \AA}$

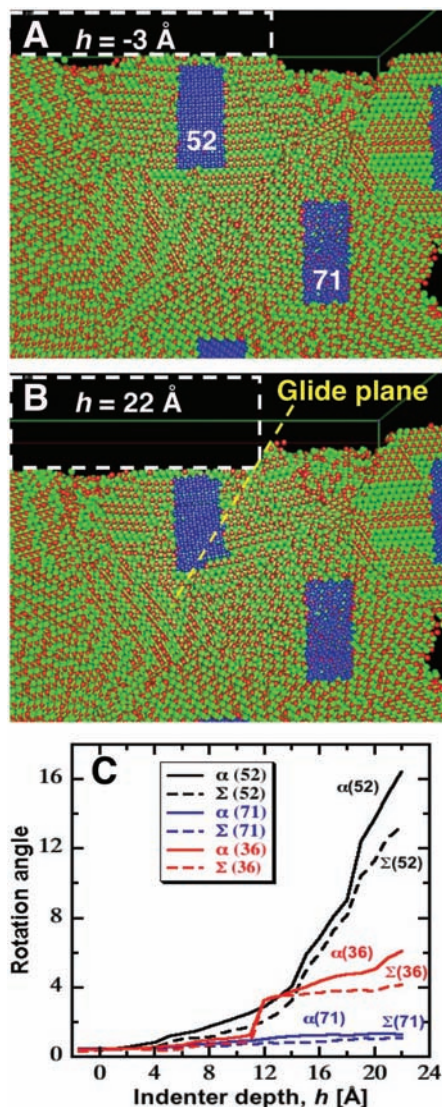


Fig. 3. Rotation of grains. (A and B) Si (green) and C (red) atoms shown in regimes 1 (A) and 2 (B) (white dashed lines depict the position of the indenter). Grain 52 experiences enormous shear beyond h_{CR} and it undergoes large rotation and deformation. (C) Rotation angle $\alpha(n)$ and its standard deviation $\Sigma(n)$ of selected grains, $n = 52, 71$, and 36. Grain 52 undergoes large rotation and deformation (black curve). Localization of deformation is reflected in the lack of rotation of grain 71 (blue curve). Grain 36 (red curve) exhibits behavior similar to stick-slip behavior at h_{CR} .

are white, and all atoms that remain disordered in the same range are yellow. The other atoms (blue and red) undergo changes in topological order, where the two competing deformation mechanisms are: ordering (crystallization) of atoms at the edges of GBs (blue) and disordering of atoms (red) in the grains. Crystallization of n-SiC has been observed experimentally during densification in the sintering process (38), and it may be responsible for the interfacial migration and small plastic flow in regime 2 of the P - h response. Even though both mechanisms are operating in the entire range of h , there is a clear switch from deformation dominated by crystallization in regimes 1 and 2 to deformation dominated by disordering in regimes 3 and 4 (Fig. 4B), in which the fraction of disordered atoms takes the minimum value at h_{CR} . The discussed disordering of atoms has been previously shown to lead to solid-state amorphization in a bulk 3C-SiC (23).

Our estimate of n-SiC hardness (defined as maximum load divided by the cross-sectional area of the indenter) of 39 GPa is in agreement

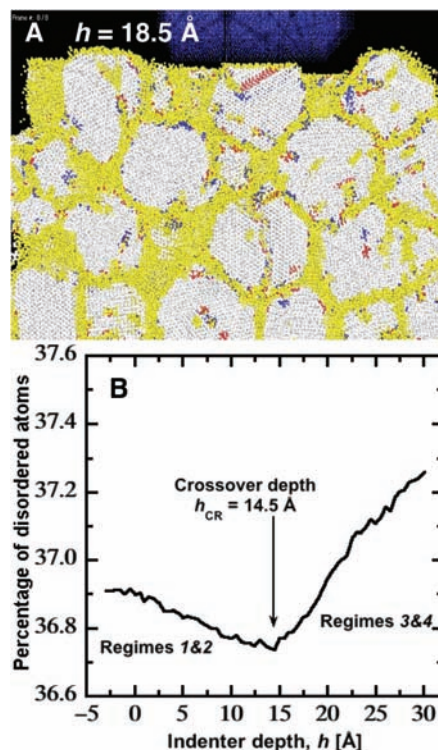


Fig. 4. Competition between crystallization and disordering in n-SiC quantified by means of shortest path ring analysis. (A) White, atoms ordered in the entire range of h up to 18.5 \AA ; yellow, atoms disordered in the entire range; blue, atoms changed from disordered to ordered (crystallized); red, atoms changed from ordered to disordered. (B) Percentage of disordered atoms as a function of indentation depth. The crossover at h_{CR} is correlated with the switch from dominating crystallization in regimes 1 and 2 to dominating disordering in regimes 3 and 4.

with experimental value of “superhardness” of 30 to 50 GPa for grain sizes of 5 to 20 nm (15). These experimental measurements are sensitive to the grain size and to the fraction of amorphous intergranular phase (15, 39, 40). This indicates an essential role of the interplay between discrete (crystalline) intragranular and continuous (amorphous) intergranular responses as a function of the length scale in determining mechanical properties, in particular for promising potential applications in advanced superhard nanostructured coatings, high-speed machining and tooling, or as potential materials for bio-implants. The two-phase character of nanostructured ceramics results in a crossover between the two aforementioned responses, and this crossover sheds light on the competition between different deformation mechanisms underlying design and fabrication of nanostructured ceramics with enhanced mechanical properties.

References and Notes

1. Y. Zhao *et al.*, *Appl. Phys. Lett.* **84**, 1356 (2004).
2. S. Zhang, D. Sun, Y. Fu, H. Du, *Surf. Coat. Technol.* **167**, 113 (2003).
3. R. W. Siegel, in *Nanomaterials: Synthesis, Properties and Applications*, A. S. Edelstein, R. C. Cammarata, Eds. (IOP, Bristol, 1996), pp. 201–218.
4. R. Madar, *Nature* **430**, 974 (2004).
5. J. Li, S. Yip, *Comput. Model. Eng. Sci.* **3**, 219 (2002).
6. J. Schiøtz, F. D. D. Tolla, K. W. Jacobsen, *Nature* **391**, 561 (1998).
7. H. V. Swygenhoven, *Science* **296**, 66 (2002).
8. S. Yip, *Nature* **391**, 532 (1998).
9. J. A. Knapp, D. M. Follstaedt, *J. Mater. Res.* **19**, 218 (2004).
10. J. Schiøtz, T. Vegge, F. D. D. Tolla, K. W. Jacobsen, *Phys. Rev. B* **60**, 11971 (1999).
11. Z. Shan *et al.*, *Science* **305**, 654 (2004).
12. D. Chen, X. F. Zhang, R. O. Ritchie, *J. Am. Ceram. Soc.* **83**, 2079 (2000).
13. P. Keblinski, S. R. Phillpot, D. Wolf, H. Gleiter, *Acta Mater.* **45**, 987 (1997).
14. P. Keblinski, S. R. Phillpot, D. Wolf, H. Gleiter, *Phys. Rev. Lett.* **77**, 2965 (1996).
15. F. Liao, S. L. Girschick, W. M. Mook, W. W. Gerberich, M. R. Zachariah, *Appl. Phys. Lett.* **86**, 171913 (2005).
16. Materials and methods are available as supporting material on Science Online.
17. D. Chen, M. E. Sixta, X. F. Zhang, L. C. D. Johnghie, R. O. Ritchie, *Acta Mater.* **48**, 4599 (2000).
18. S. Guicciardi, D. Sciti, C. Melandri, A. Bellosi, *J. Am. Ceram. Soc.* **87**, 2101 (2004).
19. W. C. Oliver, G. M. Pharr, *J. Mater. Res.* **7**, 1564 (1992).
20. J. B. Pethica, R. Hutchings, W. C. Oliver, *Philos. Mag.* **A 48**, 593 (1983).
21. W. D. Nix, *Met. Trans. A* **20A**, 2217 (1989).
22. D. Feichtinger, P. M. Derlet, H. V. Swygenhoven, *Phys. Rev. B* **67**, 024113 (2003).
23. I. Szułfarska, R. K. Kalia, A. Nakano, P. Vashishta, *Appl. Phys. Lett.* **85**, 378 (2004).
24. P. Clapp, in *Nanostructured Materials*, C. C. Koch, Ed. (Noyes, Norwich, NY, 2001), chap. 6.
25. I. Szułfarska, R. K. Kalia, A. Nakano, P. Vashishta, *Appl. Phys. Lett.* **86**, 021915 (2005).
26. A. Hasnaoui, H. V. Swygenhoven, P. M. Derlet, *Phys. Rev. B* **66**, 184112 (2002).
27. H. Hahn, K. A. Padmanabhan, *Nanostruct. Mater.* **6**, 191 (1995).
28. P. Heitjans, S. Indris, *J. Phys. Condens. Matter* **15**, R1257 (2003).
29. A. Hasnaoui, P. M. Derlet, H. V. Swygenhoven, *Acta Mater.* **52**, 2251 (2004).
30. J. Li, K. v. Vliet, T. Zhu, S. Yip, S. Suresh, *Nature* **418**, 307 (2002).
31. A. Gouldstone, H.-J. Koh, K.-Y. Zeng, A. E. Giannakopoulos, S. Suresh, *Acta Mater.* **48**, 2277 (2000).

32. W. W. Gerberich *et al.*, *Acta Mater.* **47**, 4115 (1999).
 33. A. M. Minor, J. W. Morris, E. A. Stach, *Appl. Phys. Lett.* **79**, 1625 (2001).
 34. M. Chen *et al.*, *Science* **300**, 1275 (2003).
 35. W. M. Vetter, M. Dudley, *J. Cryst. Growth* **260**, 201 (2004).
 36. A. T. Blumenau *et al.*, *J. Phys. Condens. Matter* **14**, 12741 (2002).
 37. J. P. Rino *et al.*, *Phys. Rev. B* **70**, 045207 (2004).
 38. M. Ohyanagi *et al.*, *Scripta Mater.* **50**, 111 (2004).
 39. I. A. Ovid'ko, *Science* **295**, 2386 (2002).
40. D. Wolf, V. Yamakov, S. R. Phillpot, A. Mukherjee, H. Gleiter, *Acta Mater.* **53**, 1 (2005).
 41. We thank R. Kalia, D. Morgan, and S. Babcock for fruitful discussions and H. van Swygenhoven for valuable comments on the study. This work was partially supported by Air Force Office of Scientific Research–Defense University Research Initiative on Nanotechnology, Army Research Office Multidisciplinary University Research Initiative, Defense Advanced Research Projects Agency–Predicting Real Optimized Materials, the U.S. Department of Energy,

and NSF. I.S. is supported by NSF grant DMR-0512228.

Supporting Online Material

www.sciencemag.org/cgi/content/full/309/5736/911/DC1

Materials and Methods

Fig. S1

References

4 May 2005; accepted 6 July 2005

10.1126/science.1114411

Characterization of Excess Electrons in Water-Cluster Anions by Quantum Simulations

László Turi,¹ Wen-Shyan Sheu,² Peter J. Rossky^{3*}

Water-cluster anions can serve as a bridge to understand the transition from gaseous species to the bulk hydrated electron. However, debate continues regarding how the excess electron is bound in $(\text{H}_2\text{O})_n^-$, as an interior, bulklike, or surface electronic state. To address the uncertainty, the properties of $(\text{H}_2\text{O})_n^-$ clusters with 20 to 200 water molecules have been evaluated by mixed quantum-classical simulations. The theory reproduces every observed energetic, spectral, and structural trend with cluster size that is seen in experimental photoelectron and optical absorption spectra. More important, surface states and interior states each manifest a characteristic signature in the simulation data. The results strongly support assignment of surface-bound electronic states to the water-cluster anions in published experimental studies thus far.

Clusters are widely studied, both for their direct role in atmospheric and interstellar chemistry and for their intermediacy between gaseous and condensed phases, which renders them useful simplifying models for complex molecular processes in solution. Negatively charged water clusters have long been used as models to understand the hydrated electron in bulk water. Since its discovery in 1962 (*1*), the hydrated electron has been the subject of numerous experimental (*2–5*) and theoretical (*6–10*) studies for its wide-ranging role in chemical and biological electron transfer. A consistent physical picture of its structural, spectral, and dynamic properties has emerged, bolstered in part by details extracted from clusters (*11–26*). However, a key issue remaining with regard to the cluster data is whether the electron is bulklike, trapped in the cluster interior by oriented solvent molecules, or stabilized in a surface-bound state specific to the cluster environment. This issue bears critically on the relation of cluster observations to bulk properties and the transition from one regime to the other.

Here, we address the question through mixed quantum-classical molecular simulation, which allows the direct computation of the experimental observables for these clusters. We show that the available experimental energetic and spectral data are completely consistent with the conclusion that the anionic water clusters observed to date bind the excess electron on the surface, although the long-anticipated spontaneous transition to interior states is indicated for clusters in the range of 100 to 200 molecules.

Barnett *et al.* first identified surface states through a series of quantum mechanical simulations of negatively charged water clusters (*11*). For their model, they found that clusters comprising approximately 8 to 32 water molecules bind the excess electron preferentially in a localized state on the cluster surface. The calculations predicted transition to compact hydrated electron-like interior states with increasing cluster size ($32 < n < 64$). These observations parallel the later theoretical discovery by Berkowitz and co-workers (*27*) that polarizable atomic anions preferentially adopt surface states in clusters as well (*27–29*).

Experiments have provided indirect insight into the electronic structure. The comprehensive studies of photoelectron spectra in cluster-size-selected molecular beams by Coe *et al.* (*15*) led to an excellent correlation of the most probable vertical detachment energy [(VDE), the energy needed to remove an electron at the anion's geometry] with the cluster size, n ,

through the largest cluster measured, $n \leq 69$. For clusters of $n \geq 11$, the spectroscopic data fit well to a simple linear relationship in $n^{-1/3}$ for the size dependence, based on a dielectric model assuming interior states (*11*). Because the correlation line extrapolated to a value for the infinite cluster that was consistent with simulation of bulk solvated electrons in ambient water, the authors concluded that these clusters were consistent with hydrated electron-like interior states.

However, in an important theoretical work, Makov and Nitzan developed a continuum dielectric model to evaluate the energy and free-energy differences between solvation of a spherical ion (or electron) in the center versus on the surface of a spherical solvent cluster and also estimated the VDEs (*13*). For an ion of constant radius in a solvent with high dielectric constant, they showed that the free energy of transfer between the surface and interior of the cluster essentially vanishes. The VDE of a surface state for a negative ion was actually found to be slightly larger than for an ion at the center of the solvent shell. We note that for an electron that is expectedly more delocalized at the surface than in the interior, this difference should be compensated (or possibly overcompensated, thus reversing the VDE ordering). In addition, Makov and Nitzan showed that both interior and surface states manifest the linear scaling of the VDE with $n^{-1/3}$ seen experimentally, so that this scaling did not distinguish the excess electron-binding morphologies (*13*). Of particular importance, for the infinite cluster, both surface and interior states will therefore extrapolate to the same bulk limit. Hence, the experimental observation of an extrapolated value close to the bulk does not a priori distinguish between surface and interior states.

Later, Ayotte and Johnson (*16*) measured cluster-size-selected optical absorption spectra by photodestruction. The spectral peak positions also shift linearly with $n^{-1/3}$, consistent with an excited-state energy that also scales with cluster radius. The authors noted that the excited-state VDE slope was implicitly smaller than the ground-state slope, a result that would be in harmony with different radii for the excited and ground states. The energy gap between the ground and the excited states increased with cluster size, in accord with a contracting radius. They pointed out that, of the earlier simulated energies (*11*), those for interior states were quantitatively closer to the

¹Eötvös Loránd University, Department of Physical Chemistry, Budapest 112, Post Office Box 32, H-1518, Hungary. ²Department of Chemistry, Fu-Jen Catholic University, Taipei, Taiwan 242, ROC. ³Department of Chemistry and Biochemistry, Institute for Theoretical Chemistry, University of Texas at Austin, Austin, TX 78712–1167, USA.

*To whom correspondence should be addressed. E-mail: rossky@mail.utexas.edu